Composites: Part B 68 (2015) 424–430

Contents lists available at ScienceDirect

Composites: Part B

journal homepage: www.elsevier.com/locate/compositesb

Damage classification in carbon fibre composites using acoustic emission: A comparison of three techniques

John P. McCrory [a,*], Safaa Kh. Al-Jumaili [a,c], Davide Crivelli [b], Matthew R. Pearson [a], Mark J. Eaton [a], Carol A. Featherston [a], Mario Guagliano [b], Karen M. Holford [a], Rhys Pullin [a]

[a] Cardiff School of Engineering, Cardiff University, Cardiff, Wales, United Kingdom
[b] Department of Mechanical Engineering, Politecnico di Milano, via La Masa, 1, 20156 Milano, Italy
[c] University of Basrah, Basrah, Iraq

ARTICLE INFO

Article history:
Received 31 May 2014
Received in revised form 22 July 2014
Accepted 26 August 2014
Available online 6 September 2014

Keywords:
A. Carbon fibre
B. Buckling
C. Damage mechanics
D. Acoustic emission

ABSTRACT

Classifying the type of damage occurring within a structure using a structural health monitoring system can allow the end user to assess what kind of repairs, if any, that a component requires. This paper investigates the use of acoustic emission (AE) to locate and classify the type of damage occurring in a composite, carbon fibre panel during buckling. The damage was first located using a bespoke location algorithm developed at Cardiff University, called delta-T mapping. Signals identified as coming from the regions of damage were then analysed using three AE classification techniques; Artificial Neural Network (ANN) analysis, Unsupervised Waveform Clustering (UWC) and corrected Measured Amplitude Ratio (MAR). A comparison of results yielded by these techniques shows a strong agreement regarding the nature of the damage present in the panel, with the signals assigned to two different damage mechanisms, believed to be delamination and matrix cracking. Ultrasonic C-scan images and a digital image correlation (DIC) analysis of the buckled panel were used as validation. MAR's ability to reveal the orientation of recorded signals greatly assisted the identification of the delamination region, however, ANN and UWC have the ability to group signals into several different classes, which would prove useful in instances where several damage mechanisms were generated. Combining each technique's individual merits in a multi-technique analysis dramatically improved the reliability of the AE investigation and it is thought that this cross-correlation between techniques will also be the key to developing a reliable SHM system.

1. Introduction

With the increasing use of composite materials throughout the civil aerospace and renewable energy sectors the need for structural health monitoring (SHM) of composite structures has never been more apparent [1,2]. SHM describes a method of continuously monitoring a structure for damage or decay through the use of permanently mounted or embedded sensors. A reliable SHM system would allow a structure to operate for longer between planned, routine manual inspections resulting in less downtime and hence lowering the costs associated with maintenance over the course of the service life. Being aware of the integrity of a structure throughout the entirety of its use is also inherently safer than inspecting its condition at intervals. Thus, an SHM system would be best suited for use on safety critical structures, to grant a user real-time feedback of that structure's condition, or on traditionally hard to access structures. A fully autonomous SHM system has yet to be realised, though extensive work and research is being undertaken in order to reach this goal.

One of the necessities for an effective SHM system is the ability to detect damage as it occurs, a demand which could be satisfied by acoustic emission (AE). AE is a passive method of monitoring which makes use of the elastic energy released when a material undergoes a change at the atomic scale, such as plastic deformation or cracking. Piezoelectric sensors attached to the surface of the structure detect the surface waves caused by these events and produce a voltage output. Signals which reach any sensor with an amplitude greater than a user defined threshold are recorded and subsequently stored on an AE acquisition system. A detailed explanation of AE can be found in the NDT Handbook [3]. One of the advantages of AE is its ability to identify the location of damage

* Corresponding author. Tel.: +44 2920875924.
E-mail addresses: mccroryjp@cardiff.ac.uk (J.P. McCrory), al-jumailisk@cardiff.ac.uk (S.Kh. Al-Jumaili), davide.crivelli@polimi.it (D. Crivelli), pearsonmr@cardiff.ac.uk (M.R. Pearson), eatonm@cardiff.ac.uk (M.J. Eaton), featherstonca@cardiff.ac.uk (C.A. Featherston), mario.guagliano@polimi.it (M. Guagliano), holford@cardiff.ac.uk (K.M. Holford), pullinr@cardiff.ac.uk (R. Pullin).

http://dx.doi.org/10.1016/j.compositesb.2014.08.046
1359-8368/

through the use of a sensor array and studies have been carried out to increase the accuracy with which this is done [4–6]. Further to this AE also offers the ability to classify the mechanism(s) of the damage occurring within a structure through interrogation and analysis of the waveforms collected whilst monitoring. The information contained in these waveforms, such as peak amplitude, frequency content and duration [3] could suggest the nature of the event or damage which produced them. This potential feature of AE is advantageous since accurate identification of the source mechanism of damage signals would allow the end user of an SHM system to assess what kind of repairs, if any, that a structure requires.

This paper investigates the use of three AE characterisation techniques, Artificial Neural Networks (ANN), Unsupervised Waveform Clustering (UWC) and Measured Amplitude Ratio (MAR), to classify the nature of damage occurring in a carbon fibre composite panel under a buckling regime. Validation of these methods was achieved by comparison with visual inspection and c-scanning.

2. Characterisation

The origins of damage characterisation using AE can be the traced back to 1971 [7] with the work of Mehan and Mullin [8] and Stephens and Pollock [9] and it remains a highly active area of research. Summarised by Gutkin [10], early approaches looked simply to classify damage based on a single AE parameter, such as the study by Valentin et al. [11] which used the peak amplitude of the waveforms to distinguish between matrix cracking and fibre break signals. Subsequently, to overcome the limited resolution inherent when looking at just one AE parameter, studies began to consider multiple parameters and incorporate a pattern recognition approach [12]. In addition, when AE waves travel in flat plates they exhibit a unique behaviour; the waves are bounded by the surfaces and become subject to the wave-guide effect causing them to propagate as Lamb waves [13]. Lamb waves are defined by two distinctive propagation modes; longitudinal waves, in the plane of the surface, and transverse waves, perpendicular to the plane of the surface, Fig. 1. The zero-order longitudinal and transverse modes are particularly useful as they exist across all frequencies; they are often referred to as extensional and flexural waves or S_o and A_o waves respectively.

Due to the intrinsic nature of some damage mechanisms to excite more of one Lamb wave mode than another, studies have identified the possibility of using a 'modal analysis' to classify events [15]; using the relationship between the A_o and S_o wave modes to distinguish between damage mechanisms occurring in plate like structures. In this study three characterisation methods are used and they are briefly outlined below.

2.1. Artificial Neural Network

The first pattern recognition technique employed in this study is an Artificial Neural Network analysis. This approach, described in detail by Crivelli et al. [16], is based on the work of Vesanto and Alhoniemi [17], Gunter and Bunke [18] and De Oliveira and Marques [19] and provides a completely unsupervised method for the classification of multidimensional data thus eliminating the need to specify beforehand the number of clusters present in a data set. In short, the process consists of the following steps:

1. Train a self-organising map (SOM) with AE parameters in unsupervised mode [17].
2. Cluster the trained SOM's U-matrix with the k-means algorithm [18] with m clusters, m ranging from 2 to 10.
3. Choose the best number of clusters based on the voting scheme proposed by [20] and adapted in [16].

The AE parameters used for the SOM training in this study were: rise-time, counts, absolute energy, duration, amplitude, average frequency, central frequency and peak frequency. The entire dataset is fed to the SOM, which is trained with the batch algorithm. After this phase, the trained SOM maps the n-dimensional input space (a vector of parameters extracted from each AE waveform) to the map topology space (2-dimensional). It has to be stressed that the training phase is unsupervised: no prior knowledge about the outputs is provided to the network.

2.2. Unsupervised Waveform Clustering

The second pattern recognition technique utilised is an Unsupervised Waveform Clustering analysis which is a method of using the recorded waveforms as inputs to a principal component analysis (PCA) before clustering takes place. PCA is a universally recognised method for reducing higher order data sets to lower dimensions, whilst maintaining the majority of information, or variance, within the data to allow simple analysis [21]. Described in greater detail by Nabney [22], the technique consists of interrogating multi-dimensional data to locate the two planes with maximum scatter, these give the principal components. In the field of AE the technique has previously been used as an unsupervised clustering technique to distinguish between damage and noise signals using the conventional AE features [21,23], and to separate and identify signals generated by different damage mechanisms by using the recorded waveforms as the input [24]. It has also been used to generate new uncorrelated features from conventional AE parameters for use as input vectors to clustering techniques [25,26]. However, signal attenuation over the propagation distance from the damage source to the sensor can cause conventional AE parameters to change dramatically, so a single signal can have different parameters depending on where the recording sensor is positioned [27]. To limit the clustering process' dependency on these varying parameters a segment of the recorded waveforms themselves was used as the input to the PCA, as in the study by Johnson [24], to extracted new uncorrelated features based on the waveforms' appearance. The segment of each wave analysed in the PCA was a 150 data point long sample, which is equal to 30 μs of data, starting from the first arrival of the wave. Each segment was normalised to the peak amplitude of the signal, so that the analysis only took into account the shape of the waveforms, and each segment was made to have a negative first arrival peak, to ensure all the waves were in phase. The features extracted from this PCA were subsequently used into cluster the data, using the procedure outlined below;

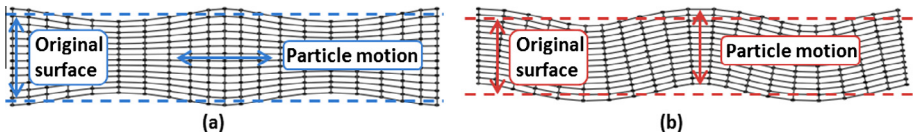

Fig. 1. (a) Longitudinal, S_o Lamb wave mode (b) Transverse, A_o Lamb wave mode [14].

1. *Mean subtraction* – Subtract the empirical mean from each column of the data set matrix.
2. *Calculate the covariance matrix* – Find the $M \times M$ empirical covariance matrix from the M dimensions data set matrix.
3. *Calculate both the eigenvectors and eigenvalues from the covariance matrix* – The directions of the first and second principal components are the same directions as the eigenvectors associated with the first and second largest eigenvalues, respectively [20].
4. *K-means clustering* – The first three high variance uncorrelated features from the PCA were used as input vectors to the k-means clustering technique.
5. Optimum cluster determination – The optimal number of clusters was determined using a Silhouette index [28].

2.3. Measured Amplitude Ratio

The modal analysis method used in this study utilises the Measured Amplitude Ratio (MAR) and works on the basis that damage which causes an out-of-plane movement of the structure, for instance delamination, will excite more energy in the flexural, A_o mode. Conversely, an in-plane movement of the structure, such as matrix cracking, will excite more energy in the extensional, S_o mode [29,30]. Thus, calculating the ratio of the S_o to A_o mode amplitudes will reveal whether the signals are S_o mode dominant (MAR > 1) or A_o mode dominant (MAR < 1) and hence suggests the nature of the damage present, i.e. in-plane or out-of-plane respectively. Using this approach previous studies have used MAR to successfully classify signals by the orientation of their source mechanism in small composite specimens [31]. However, it is understood that the attenuation of the S_o and A_o wave modes are dissimilar in carbon fibre [12,32] which is detrimental to the classification of damage using MAR on large-scale structures since the MAR will vary depending on the source to sensor propagation path. Thus a novel form of MAR calculation is proposed which corrects for the attenuation of both wave modes separately before making the amplitude ratio calculation as follows;

1. The velocities and traveling frequencies of the S_o and A_o wave modes, as well their attenuation behaviours, are established empirically in a propagation study.
2. The predicted locations of detected signals are compared to the known locations of the recording sensors to establish their propagation paths.
3. The S_o and A_o amplitudes of located signals are measured. The raw recorded signal is subjected to a band-pass filter which is designed to admit the traveling frequencies of the S_o wave mode, determined from the propagation study, thus isolating this mode and allowing its peak amplitude to be measured. This process is then repeated for a filter which admits only the A_o mode frequencies. Time of flight information is used to remove the majority of reflections before filtering.
4. The S_o and A_o amplitudes are corrected based on their predicted path and respective attenuation behaviours. This is done by dividing the amplitude of each wave mode by the amplitude of that wave mode's attenuation curve at the same propagation distance to obtain a 'correction factor'. The equation describing the attenuation curve is then multiplied by the correction factor to obtain a new attenuation equation which represents the wave mode under investigation and which can subsequently be used to obtain the amplitude of that wave mode at any propagation distance. This new equation is used to predict the amplitude of the wave mode at the source. An example of this process is shown in Fig. 2.
5. The MAR of each recorded signal is calculated after the correction of both wave modes.

3. Experimental methods

The composite panel used for this investigation was an eight ply layup of Umeco MTM44-1 unidirectional carbon fibre with the configuration $(0, 90)_{4s}$. The panel's dimensions were 403 × 376 mm with a thickness of 3.3 mm. The panel was ultrasonically C-scanned in order to assess the manufacturing quality prior to testing; no signs of damage were observed.

3.1. Propagation study

To evaluate the propagation behaviour of the S_0 and A_0 modes, four wideband, MISTRASS Group Limited (MGL) WD sensors (100–1000 kHz) were placed 70 mm apart, in a line along the 0° material direction. They were held in place between magnets positioned on both surfaces of the panel and multipurpose, brown grease was used as the acoustic couplant. The sensors were connected to MGL pre-amplifiers, set to a gain of 40 dB and with a frequency range of 20–1200 kHz, and AE data was recorded using a MGL PCI2 acquisition system. Ten Hsu–Nielsen (H–N) sources [33] were generated at a distance of 10 mm behind the first sensor and the resultant signals were recorded for all four sensors. This process was repeated at 10° intervals up to 90°.

3.2. Buckling test

The buckling test rig used for this experiment can be seen in Fig. 3. The base and the left and right edges are prevented from moving in-plane whereas the top edge is free to move vertically downwards, thus allowing the plate to be compressed by applying a force to the top edge. Roller supports along the horizontal edges

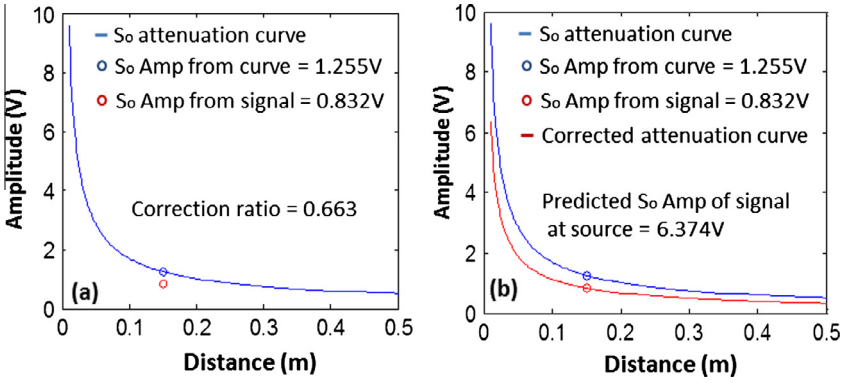

Fig. 2. Example of MAR correction process for the S_o mode of a signal recorded after 0.15 m of propagation at 50° to the fibre direction.

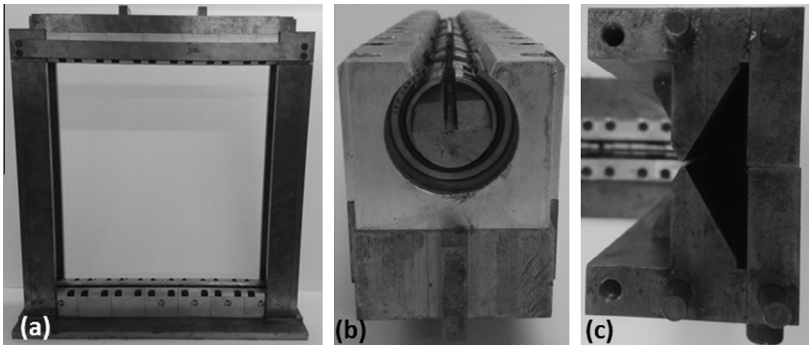

Fig. 3. (a) Buckling test rig (b) Horizontal roller supports (c) Vertical knife edge supports.

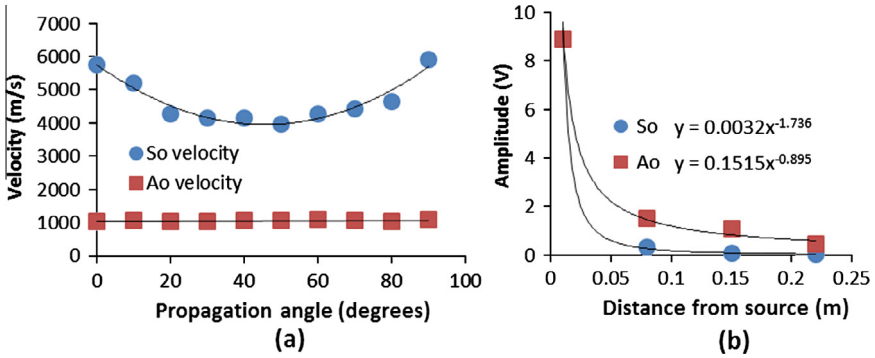

Fig. 4. (a) Velocities of propagation (b) Attenuation curves for 50° propagation angle.

and sprung knife edges along the vertical sides provide simply supported boundary conditions on all four edges.

A speckle pattern was applied to one side of the specimen, using spray paint, to allow digital imaging correlation (DIC) monitoring, a non-contact optical technique that provides full-field displacement measurements of a structure [34]. Three MGL WD sensors (100–1000 kHz) and five MGL Nano-30 sensors (125–750 kHz) were chosen to be used in the experiment; the wideband WDs were intended to extract information about the characteristics of the waveforms for the characterisation process, though due to their limited availability it was necessary to also use five Nano-30's to provide more time of arrival information and increase the accuracy of the location calculation. The eight sensors were adhered to the surface in the positions shown in Fig. 5 (a) using Loctite® 595, a multi-purpose clear silicone sealer, which also acted as the acoustic couplant between the panel and the sensors. The same AE preamplifiers and acquisition system used in the propagation study were adopted here.

The specimen was mounted into the rig and loaded in compression at a constant rate of 0.24 mm/min until failure occurred. AE data was recorded during this time and DIC images were captured manually approximately once every 1 kN of increased loading.

4. Results and discussion

4.1. Propagation study

The propagation study data was used to determine the velocities and attenuations of the S_0 and A_0 modes along each of the investigated propagation directions. Fig. 4 displays the velocities and an example of the attenuation behaviour; similar attenuation curves to these were obtained for all angles. The traveling frequencies of both wave modes in this material were also obtained through the use of a Vallen wavelet transform for each of the angles tested; these were found to be 160– > 600 kHz and 10– > 150 kHz for the S_0 and A_0 modes respectively.

4.2. Buckling test

After the specimen failed in the buckling test, it was removed from the test rig; delamination was visible by eye in the upper left corner of the panel. The test specimen was c-scanned to further assess the damage induced by loading, Fig. 5(b). A large area of high attenuation is observed in the top left corner; the four additional spots of high attenuation observed near the panel centre are caused by the panel supports.

The results of the DIC analysis revealed that the onset of buckling occurred at approximately 5 kN. During post-buckling, the panel deformed with a constant stiffness until approximately 26 kN at which point the structure's behaviour changed and the stiffness dropped, likely due to the onset of damage within the panel. Final material failure occurred at 44.61 kN.

4.3. Characterisation of AE signals

To assist the characterisation process, only located signals were analysed. Signals were located using delta-T mapping, a location algorithm developed at Cardiff University, explained in detail by Baxter [4], which can provide increased accuracy over the conventional time-of-arrival (TOA) technique [4,35]. For ease of comparison the ANN, UWC and MAR analyses were conducted using only the data recorded by the WD sensor in position 6, Fig. 5(a), because it was a wideband sensor equidistant from the two corners where AE data were recorded.

The ANN analysis identified the optimum number of clusters to be two; the AE signals that map to each cluster will be referred to

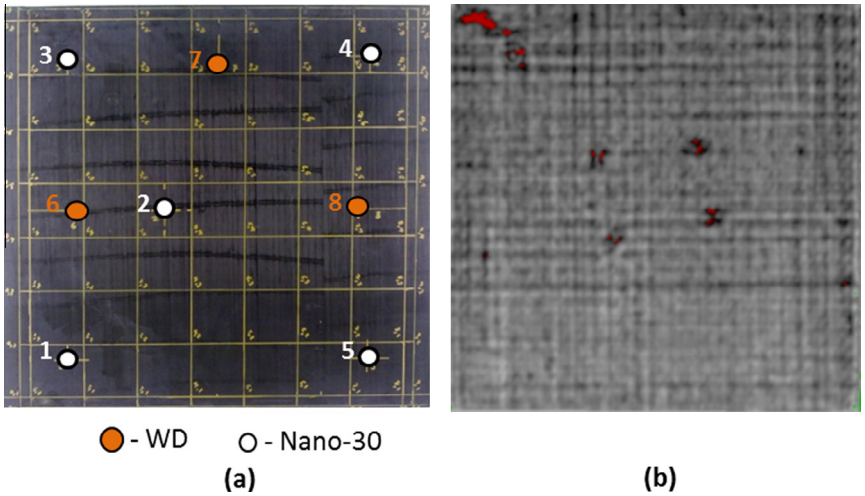

Fig. 5. (a) Delta-T mapping grid and sensor positions (b) C-scanned image after buckling.

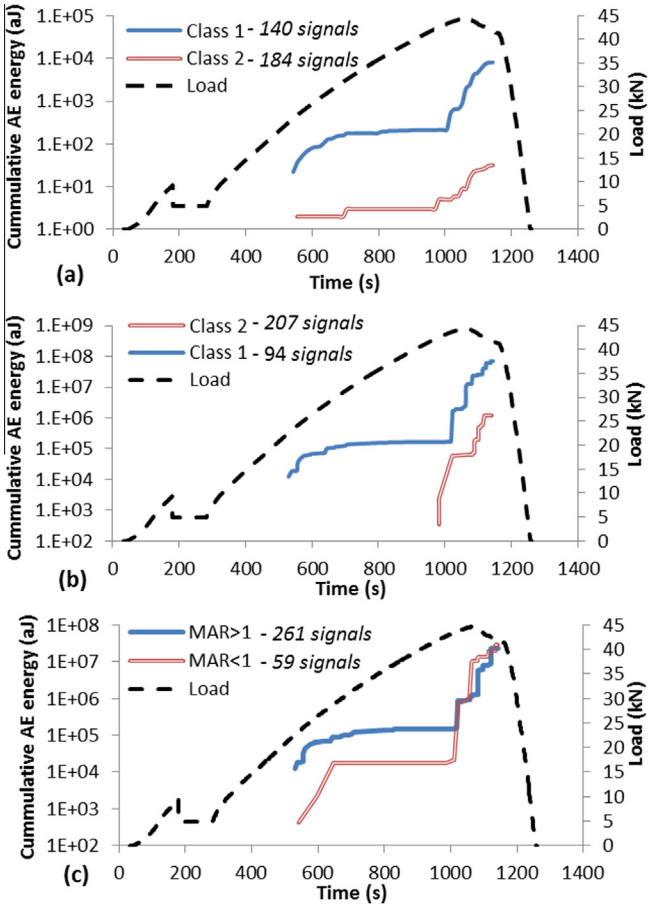

Fig. 6. Cumulate AE energy with load for (a) ANN classes (b) UWC classes (c) MAR classes.

as class 1 and class 2 from now on. The UWC also identified the presence of two unique clusters within the data set, also labelled class 1 and class 2. The MAR values calculated for the recorded waves were analysed in terms of two groups, MAR > 1 and MAR < 1, to distinguish between in-plane and out-of-plane sources respectively. Once the data was categorised by each of the techniques the cumulative energy of each class was plotted, to show the evolution of their activity over the course of the test, alongside the load trace, Fig. 6.

The cumulative AE energy curves in Fig. 6 show that there is a strong agreement between the progression of activity of the two classes between each of the characterisation methods. The drop in the load near the beginning of the test is due to the specimen settling into the test rig supports.

Class 1, as donated by ANN and UWC, and MAR > 1 signals have an earlier onset and higher overall level of activity compared with class 2 and MAR < 1 signals. There are two main periods during which class 1 and MAR > 1 signals are most active; firstly at approximately 580 s, corresponding to the point at which the DIC analysis identified the panel's stiffness to change, at 26 kN, and secondly in the period shortly before and during final failure. Class 2 and MAR < 1 signals appear in greatest abundance towards the later stages of loading, shortly before and during the final failure of the material, though there is a small amount of activity from ANN Class 2 and MAR < 1 signals (4 hits of each) before this. Thus, despite differences in the individual sums of energy of each class, the trends observed between the three classification methods are similar.

Based on the data from these plots, the test was divided into 4 time segments as follows:

- Segment 1 from 0 s to 570 s (from the beginning, to the appearance of the first located events);
- Segment 2 from 570 s to 1000 s (up to the beginning of the second class 1 high-activity phase);
- Segment 3 from 1000 s to 1070 s (the onset of the class 2 high activity phase and peak load);
- Segment 4 from 1070 s to the end of the test and final material failure;

Combining the classification of signals with the delta-T mapping location results allows the hits belonging to each class to be plotted spatially; this was done for each time segment in order to show the evolution of classified signals spatially over time. Fig. 7 shows the evolution of signals classified using UWC. It can be seen that the first located signals originate from the bottom-left corner of the panel and belong class 1. As the test progresses the activity of class 1 signals increases and the first class 2 signals begin to appear in the top-left corner of the panel. After 1000 s most activity is observed in the top-left corner with both class 1 and 2 signals occurring until final failure. By the end of the test,

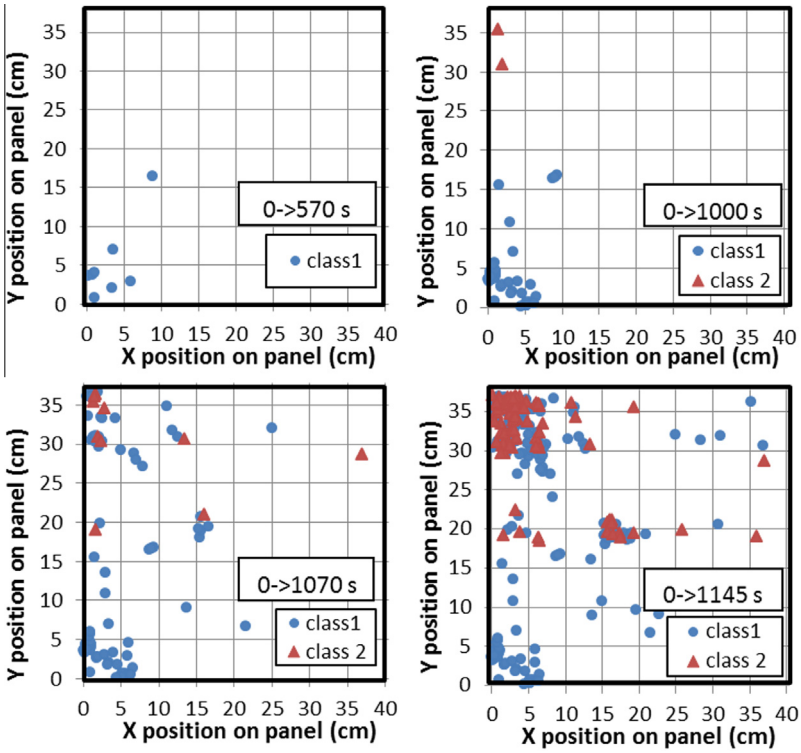

Fig. 7. Historical distribution of UWC class 1 and class 2 signals during test.

large clusters of class 1 signals can be seen to have originated from the bottom-left, centre and top-left of the panel. The majority of class 2 signals originate from the top-left corner of the panel though a small number can also be seen to originate from the centre.

Similar behaviour was observed for the ANN and MAR data, with Class 1 and MAR > 1 signals occurring initially in the bottom-left corner, followed by class 1, class 2, MAR > 1 and MAR < 1 signals occurring at the top left corner and centre in the later stages of loading.

It should be noted that the delta-T mapping location method is not without fault and it is believed that a number of signals originating from the corners were mis-located as originating from the centre of the panel. This is believed to be the case since the highest curvature in the panel is observed in the corners, where it is restrained, and so the centre of the panel, which is the least strained region, is least likely to be damaged. This mis-location effect was also witnessed on a similar, previous study [32] and so signals located as originating from the centre of the panel will no longer be discussed.

4.4. Comparison of the characterisation techniques

The ANN, UWC and MAR analyses all suggest that there are two distinct, separate sources of AE signals arising in the panel during the buckling loading regime. Each of the three techniques agree that one source is active from approximately 530 s until final failure and that the other source only features significantly after approximately 970 s, shortly before and during final failure. Finally, all three techniques agree that the AE source mechanism present towards the end of the test is most prominent in the top-left corner of the panel, whereas the source that is active throughout is more widespread, located in the bottom-left and top-left of the panel.

The C-scan inspection revealed an area of delamination at the top left corner of the panel, a common failure mode for CFRP subject to bending loads. This agrees with the result of the MAR analysis where MAR < 1 signals, indicative of delamination [29,30], are predominantly located at the top-left corner of the panel. This behaviour is also observed for the ANN and UWC analysis, where class 2 signals are predominantly located in the region of the identified delamination. Delamination is often dominant in the final failure of composite materials and hence is only likely to be present in the final stages of testing, which corresponds to the activity seen in these classes. It is believed that the ANN class 2, UWC class 2 and the MAR < 1 groups are all successfully identifying delamination damage.

Given the allocation of class 2 (ANN and UWC) and MAR < 1 signals to delamination it is likely that ANN class 1, UWC class 1 and MAR > 1 groups are identifying in-plane matrix damage. Matrix cracking is commonly the first damage mechanisms to occur in CFRPs under quasistatic loading conditions [12,19,30] and the class 1 and MAR > 1 groups are the first to appear in this test. The three classes have a large amount of activity around 600 s (26 kN) where the stiffness of the specimen was observed to change. This reduction in stiffness could be attributed to the onset of matrix damage in the material, because the matrix stiffness has a bearing on the compressive strength of composite materials [36]. The second large jump in activity of class 1 and MAR > 1 signals is around 1060 s, shortly before and during final material failure and during the onset of class 2 and MAR < 1 signals. In this instance it is likely that the curvature of the top-left of the panel, as a result of buckling and the specific restraints of the test rig, caused large enough strains for matrix cracking to take place. The build-up of this damage reduced the structural integrity of the corner until delamination occurred. This in turn caused the matrix structure to bear more of the load and crack further leading to more delamination; hence the large increase in activity of both classes of signal during final material failure. The signals belonging to ANN class 1 and UWC class 1 are less likely to be connected to fibre failure as this typically occurs closer to the final failure of the composite, as the fibres begin to exceed their ultimate strain; class 1 signals were

present throughout the test and at low loads. It is believed that fibre failure did not occur in this test to any distinguishable degree and that instead the large bending in the corners caused a tearing motion leading delamination to occur before the fibres could fail.

5. Conclusion

ANN, UWC and MAR techniques were able to successfully distinguish between different signal types arising in a carbon fibre panel subject to buckling thus leading to the characterisation of the damage occurring within the panel. This is the first time that these three techniques have been used in conjunction with one another in a collaboratively strengthened analysis. The advantage of this collaborative approach stems from the stark differences between the analysis techniques; which acted to add credibility to the result since all three techniques returned concurring results despite their different approaches. The three techniques also had their individual merits; MAR offers improved clarity during interpretation of the data, since it is inherent within the result whether a source is in or out-of-plane, which simplified the identification of the source mechanisms. ANN and UWC are advantageous in that they offer the ability to classify signals into several classes, however more interpretation of the signals in these classes is needed to determine to what mechanism they belong.

In this study the ANN, UWC and MAR approaches were used to analyse AE data collected from a buckling test on a carbon fibre panel loaded to failure. All three techniques identified two distinct classes of signal and the evolution of activity in these groups broadly agreed as the panel underwent compressive loading until failure occurred. Signals in class 1, as identified by ANN and UWC, and with MAR > 1, were attributed to matrix cracking, whereas signals in class 2, as identified by ANN and UWC, and with MAR < 1, were attributed to delamination.

The delta-T mapping location results proved to be a powerful tool when used with ANN, UWC and MAR characterisation. By providing accurate location information for each event, the classification of damage mechanisms can be achieved with greater accuracy.

Though the ANN, UWC and MAR analyses were post processed, the ever increasing performance of computing hardware means that an AE system incorporating these techniques in a live, in situ testing scenario could be realised in the near future. The ability to classify damage signals in situ would improve the capabilities of an SHM system by informing the end user of the types of damage present in a structure, though there is a great deal more work to be done making these techniques more robust and less dependent on the interpretation of the user before that goal is reached.

References

[1] Boeing. Boeing 787: from the ground up; 2008. <http://www.boeing.com/commercial/aeromagazine/articles/qtr_4_06/article_04_2.html> [12.07.13].
[2] Kensche CW. Fatigue of composites for wind turbines. Int J Fatig 2006;28(10 SPEC. ISS.):1363–74.
[3] Miller RK, Carlos MF, Findlay RD. Acoustic emission testing. In: NDT handbook, Columbus; 2005. p. 122–46.
[4] Baxter MG, Pullin R, Holford KM, Evans SL. Delta T source location for acoustic emission. Mech Syst Signal Process 2007;21(3):1512–20.
[5] Scholey JJ, Wilcox PD, Wisnom MR, Friswell MI, Pavier M, Aliha MR. A generic technique for acoustic emission. J Acoust Emission 2009;27:291–8.
[6] Eaton MJ, Pullin R, Holford KM. Towards improved damage location using acoustic emission. Proc Inst Mech Eng, Part C: J Mech Eng Sci 2012.
[7] Pappas YZ, Kontsos A, Loutas TH, Kostopoulos V. On the characterization of continuous fibres fracture by quantifying acoustic emission and acousto-ultrasonics waveforms. NDT and E Int 2004;37(5):389–401.
[8] Mehan RL, Mullin JV. Analysis of composite failure mechanisms using acoustic emissions. J Compos Mater 1971;5:266–9.
[9] Stephens RWB, Pollock AA. Waveforms and frequency spectra of acoustic emissions. J Acoust Soc Am 1971;50(3 pt 2):904–10.
[10] Gutkin R, Greena CJ, Vangrattanachaia S, Pinhoa ST, Robinsona P, Curtis PT. On acoustic emission for failure investigation in CFRP: pattern recognition and peak frequency analyses. Mech Syst Signal Process 2011;25(4):1393–407.
[11] Valentin DP, Bonniau Ph, Bunsell AR. Failure mechanism discrimination in carbon fibre-reinforced epoxy composites. Composites 1983;14(4):345–51.
[12] Sause MGR, Muller T, Horoshenkoff A, Horn S. Quantification of failure mechanisms in mode-I loading of fiber reinforced plastics utilizing acoustic emission analysis. Compos Sci Technol 2012;72(2):167–74.
[13] NDT Resource Center. Modes of sound wave propagation. <http://www.ndt-ed.org/EducationResources/CommunityCollege/Ultrasonics/Physics/modepropagation.htm> [11.07.13].
[14] Park Seismic. Multichannel approach (MASW). <http://www.masw.com/History-MASW.html> [23.08.13].
[15] Surgeon M, Wevers M. Modal analysis of acoustic emission signals from CFRP laminates. NDT and E Int 1999;32(6):311–22.
[16] Crivelli D, Guagliano M, Monici A. Development of an artificial neural network processing technique for the analysis of damage evolution in pultruded composites with acoustic emission. Compos Part B: Eng 2014;56:948–59.
[17] Vesanto J, Alhoniemi E. Clustering of the self-organizing map. IEEE Trans Neural Netw 2000;11(3):586–600.
[18] Günter S, Bunke H. Validation indices for graph clustering. Pattern Recogn Lett 2003;24(8):1107–13.
[19] de Oliveira R, Marques AT. Health monitoring of FRP using acoustic emission and artificial neural networks. Comput Struct 2008;86(3–5):367–73.
[20] Wang K, Wang B, Peng L. CVAP: validation for cluster analyses. Data Sci J 2009;8:88–93.
[21] Eaton MJ, Pullin R, Hensman JJ, Holford KM, Worden K, Evans SL. Principal component analysis of acoustic emission signals from landing gear components: an aid to fatigue fracture detection. Strain 2011;47(suppl. 1):e588–94.
[22] Nabney IT. Netlab: algorithms for pattern recognitions. In: Singh PS, editor. Springer; 2004.
[23] Calabrese L, Campanella G, Proverbio E. Noise removal by cluster analysis after long time AE corrosion monitoring of steel reinforcement in concrete. Constr Build Mater 2012;34:362–71.
[24] Johnson M. Waveform based clustering and classification of AE transients in composite laminates using principal component analysis. NDT and E Int 2002;35(6):367–76.
[25] Moevus M, Godin N, R'Mili M, Rouby D, Reynaud P, Fantozzi G, et al. Analysis of damage mechanisms and associated acoustic emission in two SiCf/[Si–B–C] composites exhibiting different tensile behaviours. Part II: unsupervised acoustic emission data clustering. Compos Sci Technol 2008;68(6):1258–65.
[26] Momon S, Godin N, Reynaud P, R'Mili M, Fantozzi G. Unsupervised and supervised classification of AE data collected during fatigue test on CMC at high temperature. Compos Part A: Appl Sci Manuf 2012;43(2):254–60.
[27] Aggelis DG, Matikas TE. Effect of plate wave dispersion on the acoustic emission parameters in metals. Comput Struct 2012;98–99:17–22.
[28] Rousseeuw PJ. Silhouettes: a graphical aid to the interpretation and validation of cluster analysis. In: Proceedings of the 2nd international conference on computational and applied mathematics. Louvain-La-Neuve, Belg; 1987.
[29] Gorman MR, Ziola SM. Plate waves produced by transverse matrix cracking. Ultrasonics 1991;29(3):245–51.
[30] Dzenis YA, Qian J. Analysis of microdamage evolution histories in composites. Int J Solids Struct 2001;38(10–13):1831–54.
[31] Eaton M, May M, Featherston C, Holford K, Hallet S, Pullin R. Characterisation of damage in composite structures using acoustic emission. J Phys: Conf Series 2011;305(1).
[32] Eaton M. Acoustic emission (AE) monitoring of buckling and failure in carbon fibre composite structures. In: Cardiff school of engineering. Cardiff University; 2007.
[33] ASTM. A standard guide for determining the reproducability of acoustic emission sensor response. Am Soc Test Mater 1994.
[34] Dantec dynamics. Measurement Principles of DIC. <http://www.dantecdynamics.com/measurement-principles-of-dic> [30.03.13].
[35] Eaton MJ, Pullin R, Holford KM. Acoustic emission source location in composite materials using Delta T Mapping. Compos Part A: Appl Sci Manuf 2012;43(6):856–63.
[36] Soutis C. Compressive behaviour of composites. In: Dolbey R, editor. Rapra Technology Limited; 1995.